RSC Advances

PAPER

View Article Online
View Journal | View Issue

Open Access Article. Published on 17 September 2025. Downloaded on 3/26/2026 2:03:08 AM.
This article is licensed under a Creative Commons Attribution-NonCommercial 3.0 Unported Licence.

Check for updates

Cite this: *RSC Adv.*, 2025, **15**, 33610

Spherical nanoflower-shaped Co-2MI with laccase-like activity for colorimetric detection of salbutamol

Lili Xu,[ab] Jianli Nan,[ac] Songxue Han,[ac] Youxing Fang*[d] and Shaojun Dong *[abc]

Received 17th July 2025
Accepted 8th September 2025

DOI: 10.1039/d5ra05134g

rsc.li/rsc-advances

A Co MOF (Co-2MI) nanozyme with uniform spherical nanoflower morphology was constructed with efficient laccase-like activity. Co-2MI displayed lower K_m and higher V_{max} than natural Laccase, indicating stronger substrate affinity and superior catalytic efficiency. Mechanistic investigations confirmed an $^{\bullet}O_2^{-}$-mediated oxidation pathway. Based on its laccase-like activity, we established a novel colorimetric method for Salbutamol detection, obtaining a linear range of 1–60 μg mL^{-1} and a low detection limit of 0.91 μg mL^{-1}. Finally, the Co-2MI nanozyme was successfully applied to the colorimetric detection of Salbutamol in real samples.

Natural laccase has demonstrated significant application potential in environmental remediation, biosensing, and various industries.[1] However, its widespread industrial use is severely limited by inherent drawbacks such as high production costs, poor stability, and difficulties in recovery.[2] To overcome these limitations, nanozymes—nanoscale materials with enzyme-mimicking activity—have emerged as promising alternatives for developing laccase-like functions.[3,4] To date, the development of laccase-mimicking nanozymes has been predominantly by copper-based materials. The catalytic activity in these systems, much like natural laccase, relies on the redox cycling of copper centers (Cu^{2+}/Cu^{+}).[5,6] This principle has been successfully applied in various designs. For instance, Yang *et al.* developed a Cu/Zn-ZIF nanozyme with superior catalytic activity by precisely simulating the copper catalytic center. Similarly, Lin *et al.* synthesized copper-based covalent organic frameworks (Cu COFs) that exhibited excellent laccase-like activity in oxidizing phenolic pollutants. These examples validate that mimicking the copper redox cycle is a highly effective strategy.[7–9] However, the principle of leveraging redox-active metal centers is not exclusive to copper.[10–12] Other transition metals with multiple valence states possess suitable redox properties that make them promising candidates for mimicking laccase activity.[13,14] Among these, cobalt is a particularly attractive candidate. Its Co^{2+}/Co^{3+} redox couple behaves similarly to copper, and cobalt-based materials often exhibit multifunctionality, opening new opportunities for biomimetic catalysis.[15,16]

To engineer these active metal centers into a highly efficient catalyst, metal–organic frameworks (MOFs) offer an ideal platform due to their tunable porous structures, high surface areas, and abundant, well-defined active sites.[17,18] The versatility of MOFs has already been demonstrated in creating laccase mimics using metals like copper, iron, and cerium.[14,19] Despite this progress, leveraging the significant potential of cobalt to develop Co MOFs as laccase mimics represents a notable and still underexplored research area. Therefore, constructing Co MOFs represents a promising and novel strategy for designing the next generation of highly efficient and stable laccase nanozymes.

Salbutamol (SAL), a β2-agonist for treating asthma, poses significant health risks upon overuse and threatens ecosystems as an emerging environmental pollutant.[20–22] Consequently, developing simple and efficient methods for monitoring SAL in environmental matrices is crucial.[23] While conventional analytical techniques like HPLC[24] and GC-MS[25] are highly sensitive, their widespread practical application is limited by high costs, complex sample pretreatment, and the need for specialized personnel. In contrast, colorimetric methods offer a promising alternative due to their simplicity, low cost, and visual detection.[26] Given that SAL is a phenolic derivative, it is a potential substrate for laccase-catalyzed oxidation. However, to our knowledge, the use of laccase-mimicking nanozymes for the colorimetric detection of SAL remains an unexplored research area.

In this study, a Co MOF (Co-2MI) nanozyme with efficient laccase-like activity was successfully designed and synthesized for the colorimetric detection of SAL. SEM and TEM characterizations revealed that Co-2MI exhibited a uniform spherical

[a]State Key Laboratory of Electroanalytical Chemistry, Changchun Institute of Applied Chemistry, Chinese Academy of Sciences, Changchun 130022, China. E-mail: dongsj@ciac.ac.cn

[b]University of Science and Technology of China, Hefei 230026, China

[c]College of Chemistry, Jilin University, Changchun 130012, China

[d]School of Chemical Engineering and Technology, Sun Yat-sen University, Zhuhai, 519082, China. E-mail: fangyouxing@mail.sysu.edu.cn

© 2025 The Author(s). Published by the Royal Society of Chemistry

Open Access Article. Published on 17 September 2025. Downloaded on 3/26/2026 2:03:08 AM.
This article is licensed under a Creative Commons Attribution-NonCommercial 3.0 Unported Licence.

nanoflower morphology. Enzyme kinetic studies showed that Co-2MI displayed a lower Michaelis–Menten constant (K_m = 0.3 mM *vs.* 4.68 mM) and higher maximum reaction rate (V_{max} = 6.23×10^{-5} mM s^{-1} *vs.* 3.58×10^{-5} mM s^{-1}) than those of natural laccase, indicating a stronger substrate affinity and superior catalytic efficiency. Mechanistic investigations using EPR and radical scavenging experiments confirmed that the catalytic process involved a $^{\bullet}O_2^-$-mediated oxidation pathway. Based on its excellent laccase-like activity, a novel colorimetric method was established for SAL detection, exhibiting a linear response range of 1–60 μg mL^{-1} and a low detection limit of 0.91 μg mL^{-1}. In spiked recovery tests with real water samples, the method showed outstanding accuracy and reproducibility, with recovery rates approaching 100% and relative standard deviations below 5%. This work first developed a Co MOF nanozyme with laccase-like activity, expanding the application scope of laccase-mimicking nanozymes in drug detection and holding significant scientific and practical value.

Co-2MI, featuring a three-dimensional (3D) nanoflower architecture assembled from two-dimensional (2D) nanosheets, was synthesized *via* a straightforward one-step solvothermal method using 2-methylimidazole (2-MI) as the organic ligand and Co^{2+} as the metal precursor. In brief, a methanolic solution of 2-MI and $Co(NO_3)_2 \cdot 6H_2O$ was heated at 120 °C for 12 h. The morphology and microstructure of the resulting Co-2MI are presented in Fig. 1. SEM images (Fig. 1a) reveal that Co-2MI assembles into a three-dimensional nanoflower architecture composed of numerous two-dimensional nanosheets. These micron-scale, layered nanoflowers offer a high specific surface area, thereby exposing abundant active sites that are beneficial for catalysis. TEM analysis (Fig. 1d) further corroborates the SEM observations, further confirming the nanosheet morphology. High-resolution TEM (HRTEM, Fig. 1f) displays clear lattice fringes with an interplanar spacing of 0.662 nm, while the selected area electron diffraction (SAED) pattern (Fig. 1e) exhibits distinct diffraction rings composed of bright spots, indicating a well-defined crystalline structure. EDX elemental mapping (Fig. 1b and c) demonstrates a uniform distribution of Co, C, O, and N throughout the Co-2MI nanoflower structure.

To further investigate the phase composition and crystalline structure of the material, X-ray diffraction (XRD) analysis was

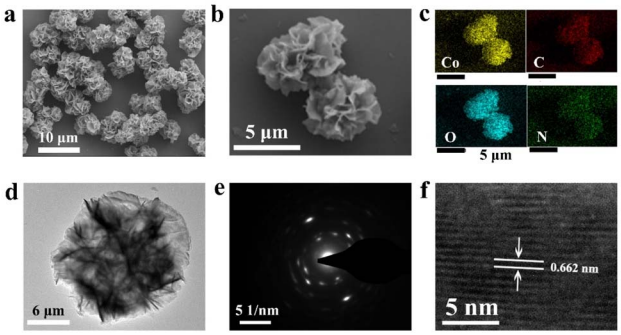

Fig. 1 (a–c) SEM and EDX elemental mapping images of Co-2MI; (d–f) TEM, SAED pattern, and HRTEM images of Co-2MI.

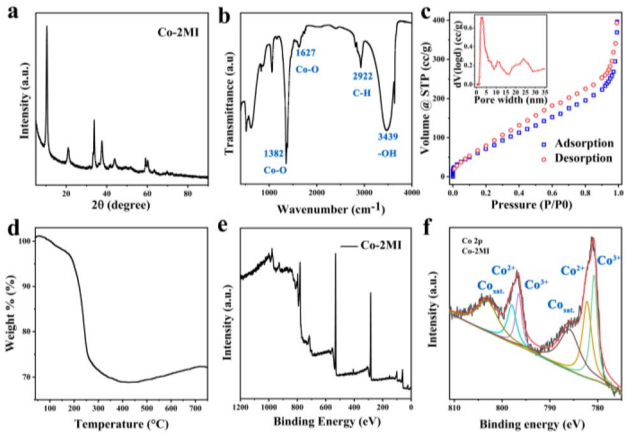

Fig. 2 (a–f) PXRD pattern, FTIR spectrum, N_2 adsorption–desorption isotherms, TGA curve, full XPS spectrum and high-resolution Co 2p XPS spectrum of Co-2MI.

performed. As shown in Fig. 2a, the XRD pattern of Co-2MI displays a characteristic diffraction peak at 10.5°, which is attributed to 2-MI within the Co-2MI framework.[27] Fourier-transform infrared spectroscopy (FTIR) was employed to probe the molecular structure and chemical composition of Co-2MI. As depicted in Fig. 2b, stretching vibrations of C–H bonds are observed at 2922 and 2852 cm^{-1}, while the broad peak at 3439 cm^{-1} corresponds to surface hydroxyl groups (–OH). The peaks at 1627 and 1382 cm^{-1} are assigned to Co–O bonds in Co-2MI.[28] Nitrogen adsorption–desorption isotherms were then used to evaluate the specific surface area and pore structure of the material. As shown in Fig. 2c, the Brunauer–Emmett–Teller (BET) surface area of Co-2MI is 316.8 m^2 g^{-1}, with an average pore diameter of approximately 7.735 nm. This indicates a high surface area and abundant porosity (Fig. S2 and Table S1). It is noteworthy that while Co-2MI possesses a significantly higher BET surface area than the other Co MOFs, the lack of any catalytic activity in the control materials suggests that the superior performance of Co-2MI is not merely a function of surface area. The thermal stability of Co-2MI was assessed using thermogravimetric analysis (TGA), as shown in Fig. 2d. X-ray photoelectron spectroscopy (XPS) was used to analyze the elemental composition and valence states. The full XPS spectrum (Fig. 2e) confirms the presence of Co, C, N, and O in the Co-2MI sample. The high-resolution Co 2p spectrum (Fig. 2f) exhibits characteristic spin–orbit doublets and satellite peaks ("Sat.") indicative of both Co^{2+} and Co^{3+} species. Specifically, peaks at 780.56 and 796.28 eV are assigned to Co^{3+}, while those at 782.03 and 797.57 eV correspond to Co^{2+}. Additionally, satellite peaks are observed at 786.11 and 802.73 eV.[29] These results suggest that Co^{3+} is the dominant species in Co-2MI, which may offer potential advantages for mimicking oxidase-like catalytic activity.

The laccase-like activity of the Co MOFs was systematically evaluated *via* the oxidative coupling colorimetric reaction between 2,4-dichlorophenol (2,4-DP) and 4-aminoantipyrine (4-AAP). To provide a benchmark for performance, natural laccase was used as a positive control for comparison against the

Open Access Article. Published on 17 September 2025. Downloaded on 3/26/2026 2:03:08 AM.
This article is licensed under a Creative Commons Attribution-NonCommercial 3.0 Unported Licence.

synthesized nanozymes under identical experimental conditions. This reaction generates a red-colored product with a characteristic absorption peak at 510 nm, where the change in absorbance directly reflects the catalytic activity. As shown in Fig. 3a, different Co MOFs exhibited significantly varied catalytic performances. Specifically, no detectable signal at 510 nm was observed for Co-BTC, Co-BDC, or Co-BPDCA, indicating they possessed negligible laccase-like activity. In contrast, Co-2MI produced a strong absorbance response far exceeding that of natural laccase, indicating its superior laccase-like catalytic efficiency. As shown in Fig. 3b, the activity of Co-2MI was several times higher than that of natural LAC under the same conditions.

To further investigate the laccase-like activity of Co-2MI, the initial reaction rates of Co-2MI and laccase catalyzing the oxidation of 2,4-DP at varying substrate concentrations were measured to evaluate their steady-state kinetics. As shown in Fig. S3a and b, the absorbance of both catalytic systems gradually increased with the rising concentration of 2,4-DP. Corresponding Michaelis–Menten curves (Fig. 3c) and the linear relationships between the initial reaction rate and 2,4-DP concentration (Fig. 3d) were obtained. Kinetic parameters K_m and V_{max} were calculated by fitting the data to the Michaelis–Menten equation. Under identical experimental conditions, Co-2MI exhibited a K_m of 0.3 mM and a V_{max} of 6.23×10^{-5} mM s^{-1}, while natural laccase showed a K_m of 4.68 mM and a V_{max} of 3.58 $\times 10^{-5}$ mM s^{-1}. The lower K_m of Co-2MI indicates a stronger substrate affinity compared to laccase, and the higher V_{max} demonstrates a faster catalytic rate. Taken together, these results clearly show that Co-2MI exhibits superior catalytic performance relative to natural laccase. The operational stability and reusability of the Co-2MI nanozyme were investigated. As shown in the SI (Fig. S6), Co-2MI maintained over 90% of its initial catalytic activity within 4 consecutive cycles of use.

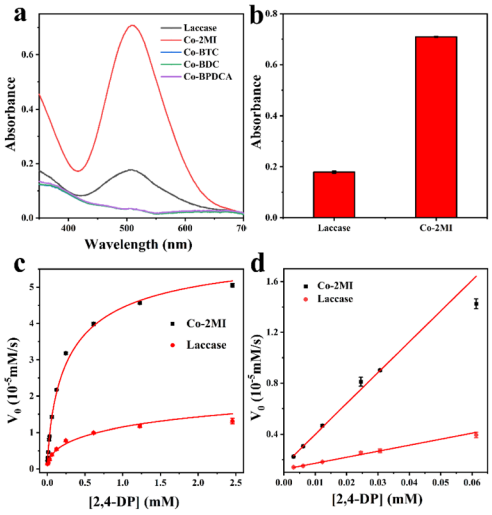

Fig. 3 (a) Spectral comparison of catalytic activity between laccase and Co MOF; (b) bar chart comparison of catalytic activity between laccase and Co-2MI; (c) Michaelis–Menten curves for 2,4-DP oxidation catalyzed by laccase and Co-2MI; (d) linear relationship between reaction rate and 2,4-DP concentration during oxidation catalyzed by laccase and Co-2MI.

To elucidate the catalytic mechanism of Co-2MI, electron paramagnetic resonance (EPR) spectroscopy was employed to identify the generation of reactive oxygen species (ROS) during the reaction. Specifically, 5,5-dimethyl-1-pyrroline *N*-oxide (DMPO) was used as a spin-trapping agent for detecting $^{\bullet}OH$ and $^{\bullet}O_2^-$, while 4-amino-2,2,6,6-tetramethylpiperidine (TEMP) was selected for detecting $^1O_2$. As shown in Fig. 4a, the EPR spectrum revealed a distinct signal corresponding to $^{\bullet}O_2^-$ in the reaction system. To further verify the role of ROS, a series of radical scavenging experiments were conducted. *tert*-Butanol (TBA), sodium azide (NaN_3), and superoxide dismutase (SOD) were used as scavengers for $^{\bullet}OH$, $^1O_2$, and $^{\bullet}O_2^-$, respectively. The results showed that NaN_3 slightly enhanced the catalytic activity of Co-2MI, TBA had a negligible inhibitory effect, while the addition of SOD significantly suppressed the catalytic activity (Fig. 4b). These findings confirm that $^{\bullet}O_2^-$ is the primary reactive species responsible for the catalytic oxidation, consistent with the EPR results. In summary, the catalytic activity of Co-2MI originates from a radical-mediated oxidation mechanism primarily involving $^{\bullet}O_2^-$.

As a fast-acting bronchodilator and lean meat agent, SAL abuse and its residues in meat can pose health risks to humans, making the quantitative detection of SAL critically important.[30,31] Characterized by its phenolic structure, SAL contains a phenolic hydroxyl group that is readily oxidized to form quinone-like structures. In this study, Co-2MI was employed to catalyze the oxidation of SAL, and the resulting oxidation products coupled with the chromogenic agent 4-AAP to generate a red-colored compound with a distinct absorption peak. Based on this mechanism, a Co-2MI-catalyzed oxidation–colorimetric detection system was developed (Fig. 5a). As shown in Fig. 5b, the absorbance intensity of the SAL oxidation-coupling product at 510 nm gradually increased with the increasing concentration of SAL.

Subsequently, Co-2MI was used to detect a series of SAL solutions at different concentrations. As illustrated in Fig. 5c, the absorbance of the oxidation–coupling product gradually increased with rising SAL concentration, reaching a plateau at higher concentrations. Within the range of 1–60 μg mL^{-1} SAL, the absorbance showed a linear correlation with SAL concentration (Fig. 5d). The detection limit, calculated at a signal-to-noise ratio of 3, was determined to be 0.91 μg mL^{-1}.

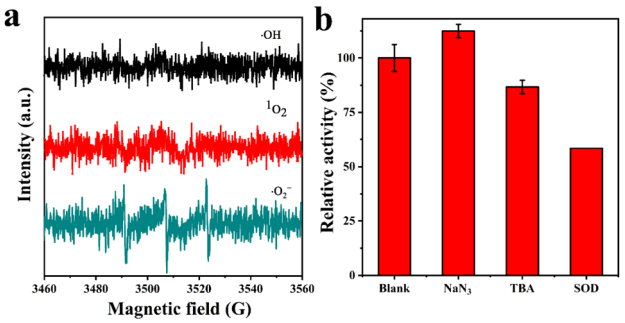

Fig. 4 (a) EPR detection of $^{\bullet}OH/^1O_2/^{\bullet}O_2^-$ with DMPO/TEMP traps; (b) 2,4-DP oxidation activity of Co-2MI with ROS scavengers (TBA/NaN_3/SOD).

 © 2025 The Author(s). Published by the Royal Society of Chemistry

Open Access Article. Published on 17 September 2025. Downloaded on 3/26/2026 2:03:08 AM.
This article is licensed under a Creative Commons Attribution-NonCommercial 3.0 Unported Licence.

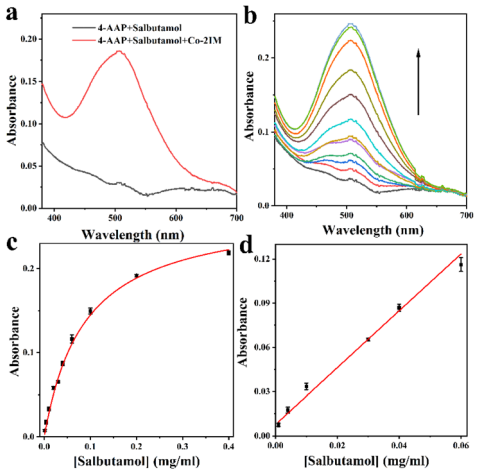

Fig. 5 (a) UV-Vis absorption spectra of SAL/4-AAP solution with/without Co-2MI; (b) absorbance changes of the reaction system with varying SAL concentrations; (c) absorbance intensity of the chromogenic system at different SAL concentrations; (d) linear relationship between absorbance intensity and SAL concentration.

Finally, this colorimetric detection system was applied to the determination of SAL in real water samples. Using a standard addition method, satisfactory recoveries were obtained, ranging from 98.3% to 101.9%, with relative standard deviations below 4.5% (Table 1), indicating the high reliability of this method for detecting SAL in practical samples. Overall, this study successfully achieved colorimetric detection of SAL by leveraging the laccase-like activity of Co-2MI.

In this work, we have reported for the first time a non-copper-based Co MOF, Co-2MI, synthesized *via* a one-step solvothermal method and exhibiting a uniform 3D nanoflower morphology assembled from 2D nanosheets. Kinetic comparisons reveal that Co-2MI has a lower Michaelis constant (K_m = 0.3 mM) and a higher maximum reaction rate ($V_{max} = 6.23 \times 10^{-5}$ mM s^{-1}) than natural laccase (K_m = 4.68 mM; $V_{max} = 3.58 \times 10^{-5}$ mM s^{-1}), indicating both stronger substrate affinity and faster catalysis. Mechanistic studies confirmed that the laccase-like oxidation follows a radical pathway with superoxide ($^{\bullet}O_2^-$) as the primary active species. Leveraging Co-2MI's robust activity, we developed a colorimetric sensor based on the Co-2MI-catalyzed oxidation of the phenolic drug salbutamol (SAL) and its coupling with 4-AAP. The assay exhibits a linear detection range of 1–60 μg mL^{-1} and a detection limit of 0.91 μg mL^{-1}, and it was successfully applied to real water samples with high recoveries. This study expands the family of laccase-mimicking nanozymes to include Co MOFs and demonstrates their promising potential in drug analysis and environmental sensing applications.

Table 1 Detection of SAL in real samples using Co-2MI

Spiked (μg mL^{-1})	Observed (μg mL^{-1})	Recovery (%)	RSD (%)
25	25.47	101.9	4.45
35	34.59	98.8	2.43
45	44.24	98.3	2.37

Conflicts of interest

There are no conflicts to declare.

Data availability

The data that support the finding of this study are available from the corresponding author upon reasonable request.

Supplementary information: Experimental section, related characterization data, and additional experimental tests. See DOI: https://doi.org/10.1039/d5ra05134g.

Acknowledgements

This work was financially supported by Science and Technology Development Plan Project of Jilin Province (SKL202302032), China and National Natural Science Foundation of China (No. 22274149 and 22074137).

Notes and references

1 I. Mateljak and M. Alcalde, *ACS Sustainable Chem. Eng.*, 2021, **9**, 9632–9637.
2 J. H. Wang, R. L. Huang, W. Qi, R. X. Su, B. P. Binks and Z. M. He, *Appl. Catal. B Environ.*, 2019, **254**, 452–462.
3 X. Li, Y. Zhang, W. L. Tan, P. Jin, P. Zhang and K. Li, *Anal. Chem.*, 2023, **95**, 2865–2873.
4 Y. H. Zhang, G. Wei, W. L. Liu, T. Li, Y. T. Wang, M. Zhou, Y. F. Liu, X. Y. Wang and H. Wei, *Nat. Rev. Methods Primers*, 2024, **4**, 36.
5 J. M. Fan, Y. J. Pu, Y. D. Wang, Y. Cui and C. Wang, *Anal. Chim. Acta*, 2025, **1336**, 343529.
6 C. Liu and Q. Huang, *Biosens. Bioelectron.*, 2025, **267**, 116784.
7 W. Y. Wei, H. Wang, P. Su, J. Y. Song and Y. Yang, *Talanta*, 2025, **291**, 127862.
8 J. Liu, C. Hu, X. Y. Meng, Y. Sun, B. Zhao and Z. Lin, *J. Hazard. Mater.*, 2025, **487**, 137142.
9 F. J. Xiao, Q. H. Xia, S. Y. Zhang, Q. L. Li, D. Chen, H. Y. Li, D. Z. Yang and Y. L. Yang, *J. Hazard. Mater.*, 2024, **465**, 133126.
10 Y. Li, Y. Dong, R. Wang, Z. Lin, J. Lin, X. Ji and B. C. Ye, *Anal. Chem.*, 2024, **96**, 2610–2619.
11 J. L. Nan, Y. Q. Liu, D. Y. Chao, Y. X. Fang and S. J. Dong, *Nano Res.*, 2023, **16**, 6544–6551.
12 J. L. Nan, Y. X. Fang, K. Rong, Y. Q. Liu and S. J. Dong, *Appl. Catal. B Environ.*, 2024, **357**, 124328.
13 L. H. Huang, Y. Tang, J. J. Wang, X. J. Niu, J. L. Zhou and Y. G. Wu, *Sensor. Actuator. B Chem.*, 2023, **391**, 134052.
14 S. Liang, X. L. Wu, J. Xiong, X. Yuan, S. L. Liu, M. H. Zong and W. Y. Lou, *Chem. Eng. J.*, 2022, **450**, 138220.
15 L. Liu, C. J. Han, G. F. Ding, M. Y. Yu, Y. F. Li, S. N. Liu, Y. X. Xie and J. Liu, *Chem. Eng. J.*, 2022, **450**, 138302.
16 M. J. Sun, R. Y. Ge, S. Li, L. M. Dai, Y. R. Li, B. Liu and W. X. Li, *J. Energy Chem.*, 2024, **91**, 453–474.
17 C. Chen, L. G. Shen, B. Y. Wang, X. C. Lu, S. Raza, J. J. Xu, B. S. Li, H. J. Lin and B. L. Chen, *Chem. Soc. Rev.*, 2025, **54**, 2208–2245.

Open Access Article. Published on 17 September 2025. Downloaded on 3/26/2026 2:03:08 AM.
This article is licensed under a Creative Commons Attribution-NonCommercial 3.0 Unported Licence.

18 K. Y. Wang, J. Q. Zhang, Y. C. Hsu, H. Y. Lin, Z. S. Han, J. D. Pang, Z. T. Yang, R. R. Liang, W. Shi and H. C. Zhou, *Chem. Rev.*, 2023, **123**, 5347–5420.
19 H. M. Qiao, H. T. Yang, Y. D. Han, Y. F. Liu, Y. Zhang and X. Zhang, *Nano Res.*, 2024, **17**, 9887–9897.
20 S. Zhao, T. Bu, K. Yang, Z. Xu, F. Bai, K. He, L. Li and L. Wang, *ACS Appl. Mater. Interfaces*, 2021, **13**, 28899–28907.
21 M. T. Gaugg, A. Engler, Y. Nussbaumer-Ochsner, L. Bregy, A. S. Stöberl, T. Gaisl, T. Bruderer, R. Zenobi, M. Kohler and P. M. L. Sinues, *J. Breath Res.*, 2017, **11**, 046004.
22 U. Armaya'u, M. M. Ariffin, S. H. Loh, W. M. A. W. M. Khalik and H. M. Yusoff, *Green Chem. Lett. Rev.*, 2022, **15**, 232–251.
23 Z. J. Liu, B. Zhang, J. F. Sun, Y. H. Yi, M. Li, D. L. Du, F. Zhu and J. W. Luan, *Sci. Total Environ.*, 2018, **613**, 861–865.
24 H. Y. Yan, R. L. Wang, Y. H. Han and S. T. Liu, *J. Chromatogr. B*, 2012, **900**, 18–23.
25 R. L. Cordell, T. S. E. Valkenburg, H. C. Pandya, D. B. Hawcutt, M. G. Semple and P. S. Monks, *J. Asthma*, 2018, **55**, 1205–1213.
26 X. F. Wang, S. S. Liu, C. J. Hou, M. Yang, J. Z. Hou, S. Y. Zhang and D. Q. Huo, *Microchem. J.*, 2024, **196**, 109576.
27 J. Luo, Y. X. Dai, X. M. Xu, Y. Z. Liu, S. G. Yang, H. He, C. Sun and Q. M. Xian, *J. Colloid Interface Sci.*, 2022, **610**, 280–294.
28 J. L. Li, L. Jiao, W. Q. Xu, H. Y. Yan, G. J. Chen, Y. Wu, L. Y. Hu and W. L. Gu, *Sensor. Actuator. B Chem.*, 2021, **329**, 129247.
29 J. Zhao, W. F. Dong, X. D. Zhang, H. X. Chai and Y. M. Huang, *Sensor. Actuator. B Chem.*, 2018, **263**, 575–584.
30 Y. J. Lei, X. Y. Li, M. S. H. Akash, L. F. Zhou, X. J. Tang, W. X. Shi, Z. M. Liu and S. Q. Chen, *J. Pharm. Biomed. Anal.*, 2015, **107**, 204–208.
31 Y. T. Wu, P. P. Dong, A. P. Deng and J. W. Di, *Anal. Methods*, 2013, **5**, 5222–5226.

 © 2025 The Author(s). Published by the Royal Society of Chemistry